NUCLEIC ACID THERAPEUTICS
Volume 32, Number 5, 2022

DOI: 10.1089/nat.2022.0009

Open camera or QR reader and scan code to access this article and other resources online.

Host-Directed Targeting of LincRNA-MIR99AHG Suppresses Intracellular Growth of *Mycobacterium tuberculosis*

Lorna Gcanga,[1–3,*] Ousman Tamgue,[1–4,*] Mumin Ozturk,[1–3] Shandre Pillay,[1–3] Raygaana Jacobs,[1–3] Julius Ebua Chia,[1–3] Stanley Kimbung Mbandi,[5] Malika Davids,[6,7] Keertan Dheda,[6–8] Sebastian Schmeier,[9] Tanvir Alam,[10] Sugata Roy,[11] Harukazu Suzuki,[11] Frank Brombacher,[1–3,12] and Reto Guler[1–3,12]

Tuberculosis (TB) caused by *Mycobacterium tuberculosis* (Mtb) kills 1.6 million people worldwide every year, and there is an urgent need for targeting host–pathogen interactions as a strategy to reduce mycobacterial resistance to current antimicrobials. Noncoding RNAs are emerging as important regulators of numerous biological processes and avenues for exploitation in host-directed therapeutics. Although long noncoding RNAs (lncRNAs) are abundantly expressed in immune cells, their functional role in gene regulation and bacterial infections remains understudied. In this study, we identify an immunoregulatory long intergenic noncoding RNA, lincRNA-MIR99AHG, which is upregulated in mouse and human macrophages upon IL-4/IL-13 stimulation and downregulated after clinical Mtb HN878 strain infection and in peripheral blood mononuclear cells from active TB patients. To evaluate the functional role of lincRNA-MIR99AHG, we used antisense locked nucleic acid (LNA) GapmeR-mediated antisense oligonucleotide (ASO) lncRNA knockdown experiments. Knockdown of lincRNA-MIR99AHG with ASOs significantly reduced intracellular Mtb growth in mouse and human macrophages and reduced pro-inflammatory cytokine production. In addition, *in vivo* treatment of mice with MIR99AHG ASOs reduced the mycobacterial burden in the lung and spleen. Furthermore, in macrophages, lincRNA-MIR99AHG is translocated to the nucleus and interacts with high affinity to hnRNPA2/B1 following IL-4/IL-13 stimulation and Mtb HN878 infection. Together, these findings identify lincRNA-MIR99AHG as a positive regulator of inflammation and macrophage polarization to promote Mtb growth and a possible target for adjunctive host-directed therapy against TB.

Keywords: *M. tuberculosis*, long noncoding RNAs, host-directed therapy, macrophages, inflammation

[1]International Centre for Genetic Engineering and Biotechnology (ICGEB), Department of Pathology, Cape Town Component, Cape Town, South Africa.
[2]Division of Immunology, Department of Pathology, Institute of Infectious Diseases and Molecular Medicine (IDM), University of Cape Town, Cape Town, South Africa.
[3]Immunology of Infectious Diseases, Faculty of Health Sciences, South African Medical Research Council (SAMRC) University of Cape Town, Cape Town, South Africa.
[4]Department of Biochemistry, Faculty of Sciences, University of Douala, Douala, Cameroon.
[5]Division of Immunology, Department of Pathology, South African Tuberculosis Vaccine Initiative, Institute of Infectious Disease and Molecular Medicine, University of Cape Town, Cape Town, South Africa.
[6]Division of Pulmonology, Department of Medicine, Centre for Lung Infection and Immunology, UCT Lung Institute, University of Cape Town, Cape Town, South Africa.
[7]South African MRC/UCT Centre for the Study of Antimicrobial Resistance, University of Cape Town, Cape Town, South Africa.
[8]Department of Infection Biology, Faculty of Infectious and Tropical Diseases, London School of Hygiene and Tropical medicine, London, United Kingdom.
[9]College of Science, School of Natural and Computational Sciences, Massey University, Auckland, New Zealand.
[10]Information and Computing Technology Division, College of Science and Engineering, Hamad Bin Khalifa University, Doha, Qatar.
[11]RIKEN Center for Integrative Medical Sciences, Cellular Function Conversion Technology Team, Yokohama, Japan.
[12]Wellcome Centre for Infectious Diseases Research in Africa, Institute of Infectious Diseases and Molecular Medicine (IDM), Department of Pathology, Faculty of Health Sciences, University of Cape Town, Cape Town, South Africa.
*These authors contributed equally to this work.

Introduction

Tuberculosis (TB), caused by *Mycobacterium tuberculosis* (Mtb), is one of the leading infectious diseases in the world [1]. In 2018, TB killed 4,110 people per day, and 27,400 people per day developed active TB globally [1]. Mtb is primarily transmitted by the respiratory route, and while it is able to cause disease in most organs, the most common involves the lungs [2]. New insights that target the host–pathogen interaction are crucial in the context of Mtb where there is a rise in antimicrobial resistance against the current 6 month regiment [3]. Mtb is able to utilize cellular host factors for its own survival and persistence [3]. Targeting these host factors exploited by Mtb could lead to a reduction in pathology, mycobacterial burden, and possible latency [3]. Long noncoding RNAs (lncRNAs) have recently emerged as regulators of transcriptional programming to alter innate and adaptive immune responses [4].

LncRNAs are a family of noncoding RNAs mainly characterized as transcripts >200 nucleotides [5,6]. LncRNAs are known to act through post-transcriptional mechanisms targeting the splicing, stability, or the translation of host mRNAs [7]. LncRNAs can act in *cis*- and *trans*- to regulate nearby genes or genes at other genomic locations [8–10]. Both *cis*- and *trans*-acting lncRNAs can activate or repress transcription through the recruitment of chromatin modifiers [8,9]. The role of lncRNAs has gained focus in recent years due to their importance in regulating macrophage biology [11–13]. For example, long intergenic noncoding RNA (lincRNA) *lincRNA-EPS* is an inhibitor of immune response gene (IRG) expression, acting as a regulatory checkpoint that is downregulated before inducible expression of IRGs [14]. The FANTOM 6 project has recently functionally annotated 285 human lncRNAs through molecular phenotyping [15]. Many other lncRNAs, including *lincRNA-Cox2* [16], *THRIL* [17], *Mirt2* [18], and *lnc13* [19], also regulate inflammatory genes in myeloid cells.

Recent studies have identified the functional role of lncRNAs during Mtb infection, which further implicated lncRNAs in immune responses [20–22]. A recently published review article has summarized recent literature on differentially expressed lncRNAs and how they regulate the immune response to Mtb infection [23]. During active TB, *lncRNA-CD244* was highly expressed in $CD244^{+}CD8^{+}$ T cells and acted as an epigenetic regulator of IFNγ and TNF-α expression by $CD8^{+}$ T cells impacting $CD8^{+}$ T cell immunity against active Mtb infection [22]. *NEAT1* was highly expressed in peripheral blood mononuclear cells (PBMCs) from patients with active TB compared to healthy individuals [24]. Knockdown of *NEAT1* resulted in increased mycobacterial growth in infected THP1 cells [24]. The expression of lincRNA-Cox2 was induced in macrophages infected with Mtb, and knockdown of lincRNA-Cox2 reduced NF-κB and STAT3 while increasing apoptosis [25]. *LncRNA-MEG3* was shown to contribute to mycobacteria clearance in macrophages infected with *Mycobacterium bovis* BCG through autophagy by targeting the mTOR and PI3K-AKT signaling pathways [21].

A microarray study examined expression profiles of lncRNAs in human macrophages infected with virulent H37Rv Mtb and avirulent H37Ra strains. Two lncRNAs *MIR3945HG V1* and *MIR3945HG V2* were identified as novel candidate diagnostic markers for TB [26]. Our understanding of the functional role of lncRNAs in M2 (IL-4/IL-13) polarized macrophages and during Mtb infection and their clinical relevance is still limited.

In this study, we identify lincRNA-MIR99AHG (hereon referred to as MIR99AHG) to be abundantly expressed in M2 (IL-4/IL-13) polarized mouse and human monocyte-derived macrophages (MDMs) and downregulated in PBMC from active TB patients and Mtb HN878 infected mouse and human macrophages. We demonstrate that MIR99AHG regulates inflammatory gene expression in macrophages stimulated with IL-4/IL-13 and infected with the clinical Mtb HN878 strain. Using antisense oligonucleotides (ASOs) lncRNA knockdown approaches, we show that knockdown of MIR99AHG in Mtb infected mice reduced mycobacterial burden in the lung and spleen. Mechanistically, we demonstrated in macrophages that MIR99AHG interacts with hnRNPA2/B1 in the nucleus following IL-4/IL-13 stimulation and Mtb HN878 infection. We propose a model whereby MIR99AHG regulates host-inflammatory response and promotes Mtb intracellular survival and persistence in macrophages.

Materials and Methods

Ethics statement

The BALB/c mouse strain was bred and housed in specific pathogen-free conditions, and all animal procedures were performed in compliance with the standards of practice for laboratory animal procedures set by the Animal Research Ethics Committee, Faculty of Health Sciences, University of Cape Town, Cape Town, South Africa (Ethics approval Ref 015/040). The recruitment of healthy volunteers for this study was approved by the Human Ethics Committee, Faculty of Health Sciences, University of Cape Town, Cape Town (HREC Ref No.: 635/2015). Inclusion criteria were as follows: age 18–50 years, both sexes, no history of TB, no contact with TB patients, HIV negative, sputum smear-negative, nonsmokers, no chronic alcoholism, normal chest X-rays, no chronic disease, not receiving immunosuppressive therapy, interferon-gamma release assay negative, and absence of other pulmonary diseases.

The participants who did not meet the above criteria, did not consent to signing the information consent form, or to undertaking an HIV test were excluded from this study. The recruitment of active TB patients for this study was approved by the Human Ethics Committee, Faculty of Health Sciences, University of Cape Town, Cape Town (HREC Ref No.: 624/2015). Inclusion criteria were as follows: Informed consent, culture-positive individuals (aged 18–50 years), chest X-ray consistent with proven pulmonary TB and without prior TB treatment, sputum smear-positive, and HIV negative.

Mice

Wild-type BALB/c and IL-$4R\alpha^{-/-}$ on a BALB/c background mouse (8–10 weeks) were housed under specific pathogen-free conditions in individually ventilated cages.

Generation of bone marrow-derived macrophages

Bone marrow-derived macrophages (BMDMs) were generated from 8- to 11-week-old male BALB/c mice. The mice were sacrificed using halothane and death was confirmed by cervical dislocation, and their femur bones were flushed

using plain Dulbecco's modified Eagle's medium (DMEM; Gibco, Invitrogen Corporation, Carlsbad, CA, USA) to collect (centrifugation: 1200 rpm; 4°C; 10 min) bone marrow cells. The cells were seeded in sterile 100 mm CORNING plates (14×10^6 cells/mL) and incubated [37°C; 5% carbon dioxide (CO_2); 70% relative humidity (RH)] for 10 days in PLUTZNIK media [DMEM containing 10% fetal calf serum (FCS), 5% horse serum, 2 mM *L*-glutamine, 1 mM sodium pyruvate, 0.1 mM 2-beta-Mercaptoethanol, 30% L929 cell-conditioned medium, 100 U/mL penicillin G, 100 µg/mL streptomycin] to allow for their differentiation into BMDMs.

On day 10, the adherent cells were lifted using 4 mg/mL Lidocaine ethylenediaminetetraacetic acid (EDTA) solution and gentle scrapping, thereafter, washed twice with DMEM (containing 10% FCS, 100 U/mL penicillin G, 100 µg/mL streptomycin) to remove residual M-CSF (present in the L929 conditioned medium). The BMDMs were seeded at 2–3×10^6 cells/well, 5×10^5 cells/well, and 1×10^5 cells/well in 6, 24, and 96-well Nunc plates, respectively, and incubated (37°C; 5% CO_2; 70% RH) overnight before performing downstream experiments.

Generation of PBMCs and MDMs

PBMCs were isolated using Histopaque®-10771 (Sigma-Aldrich Biotechnology LP and Sigma-Aldrich Co., St Louis, MO, USA) density gradient centrifugation. Blood was collected in VACUETTE® K3E blood collection tubes (Greiner Bio-one, GmbH, Germany), transferred to 50 mL Falcon tubes, and diluted 1:2 with isotonic phosphate buffered saline (PBS) solution pH 7.4. Thirty milliliters of diluted blood was transferred to 50 mL Leucosep™ 227290 tubes (Greiner Bio-one, GmbH) loaded beforehand with 15 mL Histopaque solution as per the manufacturer's instructions. The tubes were centrifuged at 1,000 *g* (2,229 rpm) for 25 min (acceleration: 9; deceleration: 0) using an Eppendorf® 5810R centrifuge (A-4-81 Rotor, radius 18 cm). Plasma was discarded, and buffy coat (lymphocytes/PBMCs) layer was harvested into a fresh 50 mL Falcon tube. The buffy coat was washed thrice with 50 mL PBS solution pH 7.4 and spun at 250 *g* for 10 min (acceleration 9, deceleration 5). PBMCs were resuspended in 2–5 mL complete growth medium [Roswell Park Memorial Institute (RPMI) 1640 medium supplemented with 10% FCS, 2 mM *L*-glutamine, and 1% penicillin G/streptomycin; all purchased from Life Technologies™, Carlsbad, CA, USA]. PBMCs were plated at 1×10^5 cells per 96-well tissue culture plates (Corning Costar®, Cambridge, MA, USA) in complete growth medium for downstream bacterial burden experiments. For the generation of MDMs, PBMCs were plated in 6-/12-/96-well tissue culture plates (Corning Costar) at a density of $20/10/1 \times 10^6$ cells/well, respectively, and incubated (37°C; 5% CO_2; 70% RH) for 2 h to allow monocytes to adhere. Nonadherent cells were discarded, and adherent monocytes were given a gentle wash with PBS then incubated in X-VIVO™ 15 serum free hematopoietic medium (supplemented with 1% penicillin G/streptomycin) for 7 days to allow for the differentiation of monocytes into MDMs. X-VIVO 15 serum free hematopoietic medium was changed on day 4. On day 7, X-VIVO 15 was removed, MDMs washed once with PBS, and complete growth medium added for downstream experiments. MDM purity was assessed by fluorescence-activated cell sorting (FACS) analysis using a PE-labeled anti-CD11b; PerCP-labeled anti-HLA-DR; FITC-labeled anti-CD14, and APC-labeled anti-CD3 monoclonal antibodies (All purchased from BD Biosciences™, CA, USA). MDM purity exceeded 95%.

ASO synthesis and purification

ASOs used in this study were synthesized by Exiqon™/Qiagen, Germany. All ASOs, including scrambled GapmeR negative control, are 16 nucleotides in length and chemically modified with phosphorothioate backbone. The locked nucleic acid (LNA) GapmeRs were designed to provide potent and specific target knockdown. The primary design parameters include: (1) optimal target sequence accessibility to ensure high potency by selecting target sequences based on local secondary structure prediction, (2) antisense off-target evaluation by aligning GapmeR sequences against ENSMBL to allow selection of the most specific antisense LNA GapmeRs with minimal off-targets, and (3) optimal ASO design, including length, melting temperature, self-complementarity, LNA positions. The product sequences of ASOs used in the study are GAP-MIR99AHG 5′-CAGTTGCGTGGAGTAA-3′, GAP-MIR99AHG, 5′-CTAGCTTTGAAGTCGT-3′, GAP-hsMIR99AHG 5′-CAGTTGCGTGGAGTAA-3′ and scrambled GapmeR negative control 5′-AACACGTCTATACGC-3′.

The ASOs were purified and analyzed by electrospray ionization mass spectrometry (ESI-MS) using anion-exchange high performance liquid chromatography, desalted and lyophilized as a sodium salt. The scrambled GapmeR negative control used in the study has the same chemical composition to target ASO-MIR99AHG. Purity and mass of oligonucleotides were confirmed by ESI-MS with more than 80% purity guaranteed. The ASOs were resuspended in Tris-EDTA buffer, sterile and filtered, and added to the cell culture medium.

Transfection of BMDMs and MDMs by ASOs

Antisense LNA GapmeR targeting (Exiqon/Qiagen, Germany) MIR99AHG was diluted in Opti-MEM medium (Life Technologies) and mixed in a 1:1 ratio with Lipofectamine RNAiMAX 3000 (Life Technologies). As a negative control, nontargeting scrambled LNA GapmeR (Exiqon/Qiagen, Germany) was transfected to the macrophages. For mouse and human macrophage cultures, two GapmeR MIR99AHG designs (5′- CAGTTGCGTGGAGTAA-3′ and 5′-CTAGCTTT GAAGTCGT-3′) were used to transfect murine macrophages, and for the *in vivo* experiment in mice one GapmeR MIR99-AHG design was used (5′-CAGTTGCGTGGAGTAA-3′).

Cultured cells were transfected with 25 nM of GapmeR for 48 h, and the medium was replaced with DMEM or RPMI medium supplemented with 10% FCS for downstream experiments. *In vitro* dose–response experiments were performed to optimize ASO transfections, investigating the effect of different concentrations of scrambled GapmeR negative control on BMDM cell viability. BMDMs treated with scrambled GapmeR negative control for 24, 48, or 72 h at either 10 or 50 nM did not cause any cell toxicity in cell culture plates seeded with 200,000 macrophages as confirmed by CellTiter Blue assay (Supplementary Fig. S4A–C).

Stimulation with M. tuberculosis, M. bovis *BCG, and* Leishmania mexicana *on BMDMs and MDMs*

Macrophages were stimulated with recombinant mouse (100 units/mL) or recombinant human (10 ng/mL) IL-4,

IL-13, or a combination of IL-4 and IL-13 (IL-4/IL-13; BD Biosciences). At 24 h poststimulation, macrophages were infected with a frozen stock of the clinical hypervirulent Mtb HN878 and mCherry expressing H37Rv strain, *M. bovis* BCG, and with *L. mexicana* M379 strain at a multiplicity of infection (MOI) of 2 bacilli:1 cell (2:1). Beads were used to disperse clumps of mycobacteria. After 4 h, the supernatant was removed, and fresh DMEM containing 10% FCS, 100 U/mL penicillin G, 100 μg/mL streptomycin, 10 μg/mL Gentamicin with or without stimulants was added to remove extracellular bacteria. Two hours later, the medium was replaced with DMEM containing 10% FCS with or without stimulants.

RNA extraction

Cells were lysed in QIAzol (Qiagen) at different timepoints post-transfection/-stimulation/-Mtb infection, and lysates were stored at −80°C. Total RNA was isolated from the lysate using miRNeasy Mini Kit (Qiagen) according to the manufacturer's instructions. RNA quantity and purity were measured using the ND-1000 NanoDrop spectrophotometer (ThermoScientific, DE, USA).

cDNA Synthesis and Quantitative real-time polymerase chain reaction

For protein coding gene and lncRNA expression analysis, 100 ng total RNA was reverse-transcribed into cDNA using Transcriptor First Strand cDNA Synthesis Kit (Roche, Germany) according to the manufacturer's instructions. Quantitative real-time polymerase chain reaction (RT-qPCR) was performed using LightCycler® 480 SYBR Green I Master (Roche) and gene-specific primers (IDT, CA, USA). Fold change in gene expression was calculated by the ΔΔCt method and normalized to Hprt1 which was used as internal control. The fold change expression was calculated using the ΔΔCt method to the housekeeping gene (HPRT) set to 1.

Bacterial Burden Determination

At 24, 48, and 72 h postinfection, supernatant was removed from Mtb-infected macrophages and stored at −80°C for analysis of cytokine production. Cells were lysed at 4, 48, and 72 h postinfection in Triton X-100, and serial dilutions were plated on Middlebrook 7H10 agar plates and incubated for 15 days at 37°C in 5% CO_2. Colony forming units (CFUs) were enumerated to determine bacterial burden.

Cytokine production

Cytokine production was measured by enzyme-linked immunosorbent assay (ELISA) using ELISA development reagents (R&D systems, USA) at 24, 48, and 72 h post Mtb. Culture supernatants were diluted two, three, and sixfolds. Data were acquired using VersaMax™ Tunable microplate reader with SoftMax Pro v6.3. (Avantor®, USA).

Griess reagent assay

Cultured supernatants were collected at 48 h post Mtb to measure protein levels of nitrite, which correlate to nitric oxide (NO) production, by Griess reagents. Read out was acquired using VersaMax Tunable microplate reader with SoftMax Pro v6.3 (Avantor).

RNA pull-down assay

Biotin-labeled lincRNA-MIR99AHG was transcribed with biotin RNA labeling mix and T7 RNA polymerase (Promega), treated with RNase-free DNase I (Promega), and purified using RNeasy Mini Kit (Qiagen). Biotin-labeled lincRNA-MIR99AHG was mixed and incubated with nuclear extracts of IL-4/IL-13 stimulated and Mtb HN878 infected BMDMs. Streptavidin-conjugated magnetic beads (Invitrogen) were added to each binding reaction and further incubated. Beads were washed thoroughly. Retrieved proteins were detected by mass spectrometry.

RNA immunoprecipitation

HnRNPA2/B1 experiments were performed in nuclear extracts isolated from IL-4/IL-13 stimulated and Mtb HN878 infected BMDM formaldehyde cross-linked conditions. Assays were performed as described in the Novex IP Kit protocol (10007D) except that cells were crosslinked with 1% formaldehyde for 20 min. Nuclear extracts were precleared with protein G beads for 2 h at 4°C and then incubated with control rabbit IgG or anti-hnRNPA2/B1 antibody (2 μg/sample) for 2 h at room temperature. RNA was collected from 800 μL of each sample using TRIzol and treated with DNase to remove contaminating DNA. MIR99AHG levels were analyzed by real-time-qPCR. The remaining 200 μL of each sample was collected, boiled for 10 min, and subjected to Western blot analysis.

Western blot

BMDMs were harvested and lysed in RIPA buffer supplemented with protease inhibitor (P-8340, Sigma-Aldrich). Protein concentrations in cell lysates were measured using Pierce™ BCA Protein Assay Kit (23225, Thermo Fisher Scientific, USA), and the same amount of protein was loaded and separated on a polyacrylamide gel. Proteins were transferred to a nitrocellulose membrane. Membranes were blocked with 5% bovine serum albumin (BSA) solution [prepared in Tris-buffered saline, 0.1% Tween 20 (TBST)] for 2 h and probed with primary antibodies overnight in dilution buffer (TBST supplements with 1% BSA). The antibodies used in Western blots are: hnRNPA2/B1 (sc-32316; Santa cruz), hnRNPL (ab6106; Abcam), hnRNPK (sc-28380, Santa cruz), Cxadr (sc-373791, Santa cruz), and Gapdh (sc-365062, Santa Cruz). Membranes were probed with horseradish peroxidase-conjugated anti-mouse and anti-goat secondary antibodies (sc-2005 and sc-2020). Western blots were developed with LumiGLO Reserve™ Chemiluminescent Substrate Kit (54-64-01; SeraCare, Life Sciences, MA, USA).

In vivo *LNA-GapmeR ASO treatment*

Eighteen wild-type BALB/c mice randomly assigned were injected intraperitoneally with control [LNA GapmeR Negative Control A (10 mg/kg; Exiqon)] or ASO-MIR99AHG (10 mg/kg; Exiqon) for alternate days up to 14 days.

Histology

Lung sections were collected from euthanized mice and placed in 4% formaldehyde solution. Embedded sections were then stained with Hematoxylin and Eosin (H&E). The percentage of free alveolar spaces was defined as the open spaces in whole lung sections in relation to the total lung tissue area.

Both free spaces and tissue areas were measured using the area measurement tool by the Nikon Imaging Software (NIS) elements, and the percentage of alveolar spaces was calculated in Excel. A blinded quantification was performed to measure the percentage of myeloperoxidase (MPO), CD3, inducible nitric oxide synthase (iNOS), and Caspase-3 using the Nikon microscope imaging software NIS elements.

Flow cytometry and lung myeloid cell sorting

Assessment of BMDM activation into M1 or M2 state, the extent of macrophage infection with mCherry expressing Mtb, and assessment of apoptosis using Annexin V and 7-AAD staining were measured by flow cytometry. For surface staining of BMDM activation, cells were labeled with appropriate antibodies MHCII (M5/114.15.2), CD11b (M1/70), CD64 (X54–5/7.1), CD86 (GL1), CD80 (16–10A1), CD206 (C068C2), PD-L2 (TY25) purchased from BD Biosciences (Franklin Lakes, NJ, USA) and eBioscience (San Diego, CA, USA). After incubation, cells were resuspended in FACS buffer (0.1% BSA and 0.1% sodium azide in PBS) for acquisition. The acquisition was performed using BD LSRFortessa (BD Biosciences), and data were analyzed using FlowJo software V10 (Treestar, Ashland, OR, USA).

Lung myeloid cell sorting was performed from the lungs of 3 weeks HN878 infected mice. Briefly, left lung and postcaval lobes are mechanically minced before incubation in DMEM containing 0.18 mg/mL Collagenase Type I (Sigma), 0.02 mg/mL DNase I for 1 h at 37°C under rotation, followed by passing through 100 and 70 μm cell strainers sequentially. Red blood cells were lysed with lysis buffer (155 mM NH_4Cl, 12 mM $NaHCO_3$, 0.1 mM EDTA). Cells were then counted and subjected to antibody staining. The 575V Fixable viability stain, CD64 (X54–5/7.1), CD11b (M1/70), CD11c (HL3), SiglecF (E5–2440), and Ly6G (1A8) were used to stain lung myeloid cells for 20 min in 4°C. Alveolar macrophages, monocyte-derived DC, and interstitial macrophages were sorted in complete media using BD FACSAria Fusion. Cells were later spun at 400 *g* for 5 min and resuspended in QIAzol for downstream gene expression analysis. The gating strategies for flow cytometry experiments are provided in Supplementary Fig. S2A and B.

RNA sequencing

Wild-type BMDMs were transfected with LNA GapmeRs and infected with Mtb HN878 with an MOI of 1:2 for 4 and 24 h. RNA-seq libraries were prepared from total RNA and sequenced on Illumina HiSeq2000 as described [27].

Mtb infection for determination of burdens in mice and Listeria monocytogenes *infection in mice for RT-qPCR analysis*

Anesthetized mice were infected intranasally with 25 μL of viable HN878 Mtb bacilli into each nasal cavity with doses of 100 CFU/mouse for immune response analysis. Bacterial loads and histopathological and flow cytometry analyses in lungs of Mtb-infected mice were determined as previously described [28]. The lung weight index calculation was performed as a measure of inflammatory infiltration using: square root [(Lung weight in milligram/Mouse weight in gram) × 10]/10. Briefly, aseptically harvested lungs and spleen were homogenized in 0.01% Tween-PBS, and 10-fold dilutions were plated on 7H10 agar plates for the determinations of CFUs. Mice were infected intraperitoneally with *L. monocytogenes* with a high dose of 2×10^5 CFU/mouse, and liver and spleen were harvested for RT-qPCR analysis.

Cell viability and apoptosis

Assessment of apoptosis was analyzed by flow cytometry using the FITC Annexin V Apoptosis Detection Kit II (BD Biosciences). After incubation, cells were resuspended in FACS buffer for acquisition. Acquisition was performed using BD LSRFortessa (BD Biosciences), and data were analyzed using FlowJo software (Treestar). Cell viability was assessed using CellTiter Blue (Promega). After incubation, data were analyzed using VersaMax Tunable microplate reader with SoftMax Pro v6.3 (Avantor). Apoptosis of macrophages *in vitro* was assessed with the fluorescent *in situ* terminal deoxynucleotidyl transferase dUTP nick-end labeling (TUNEL) assay according to the manufacturer's specifications (*In Situ* Cell Death Detection Kit, Roche). BMDMs were incubated for 1 h with 4% paraformaldehyde at room temparature. Macrophages were washed once with 1 × PBS and incubated for 2 min on ice with a permeabilization solution (0.1% Triton X-100) and washed twice with 1 × PBS. Macrophages were labeled with the TUNEL reaction mixture for 1 h at 37°C and then analyzed with fluorescent microscopy.

Statistical analysis

All data were analyzed using GraphPad Prism v6.0, a Student's *t*-test (two-tailed with unequal variance) or unless otherwise stated in Figure legends. Means are shown as standard deviation (SD), $*P < 0.05$, $**P < 0.01$, $***P < 0.001$, and $****P < 0.0001$, respectively.

Results

MIR99AHG is upregulated in M2 (IL-4/IL-13) murine and human macrophages, downregulated following Mtb HN878 infection and dependent on the IL-4Rα pathway

We previously utilized deep CAGE (Cap Analysis of Gene Expression) transcriptomics to define the transcriptome of M1 (IFN-γ) or M2 (IL-4, IL-13, IL-4/IL-13) activated BMDMs [12,29,30] and during Mtb HN878 infection [31,32]. Using this approach (Fig. 1A, B), we identified several differentially expressed lncRNAs with MIR99AHG being highly expressed in M2 (IL-4/IL-13) stimulated macrophages (Fig. 1C). At 4 h post stimulation, IL-4/IL-13 upregulated 40-fold the expression CAGE tags per million (TPM) of MIR99AHG compared to the unstimulated macrophages. This upregulation was mediated by IL-4/IL-13 signaling using the common IL-4 receptor alpha chain, since in IL-4Rα$^{-/-}$ BMDMs, we did not induce the expression of MIR99AHG to the same levels as wild type (Fig. 1D). In contrast, Mtb HN878 infection repressed MIR99AHG expression in a time dependent manner (Fig. 1E). The CAGE TPM expression of MIR99AHG was validated by RT-qPCR in cytokine-stimulated and Mtb HN878 infected macrophages (Fig. 1F, G).

In addition, MIR99AHG was downregulated in mice infected with Mtb HN878 at 11- and 21-days postinfection (Fig. 1H). As in BMDMs, human MIR99AHG expression in

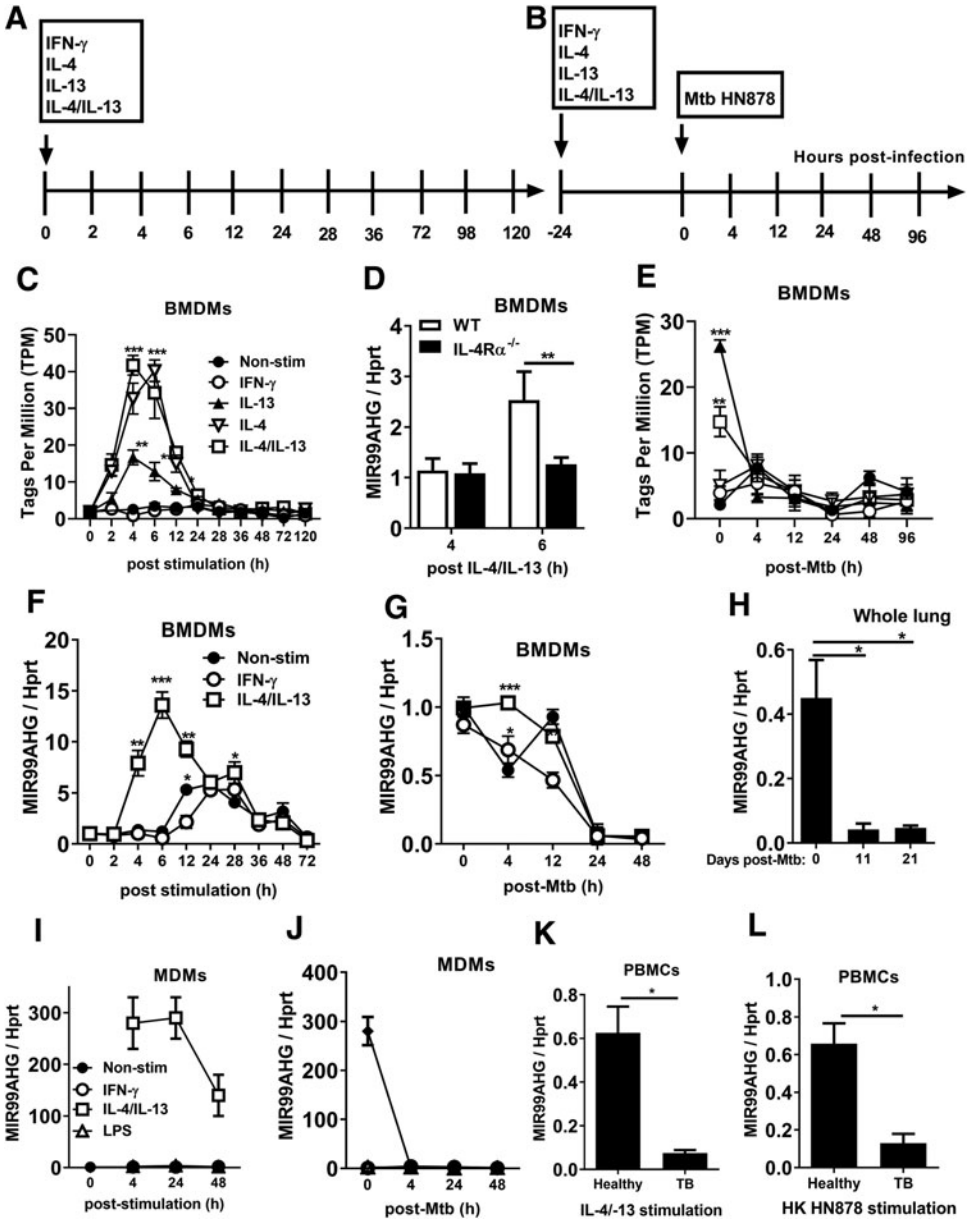

FIG. 1. MIR99AHG is upregulated in M2 (IL-4/IL-13) in murine and human macrophages, downregulated following Mtb HN878 infection, and dependent on the IL-4Rα pathway. Bone marrow cells were differentiated for 10 days into BMDMs and stimulated with IFNγ or IL-4, IL-13, IL-4/IL-13. At 24 h poststimulation, BMDMs were infected with Mtb HN878 for 4, 24, and 48 h. RNA was extracted from lysed cells at different time points poststimulation and post-Mtb HN878 infection. **(A, B)** Timeline of mouse macrophage cytokine stimulation and Mtb HN878 infection. **(C, E)** CAGE analysis of MIR99AHG TPM kinetic expression in cytokine stimulated and Mtb HN878 infected BMDMs. Data are representative of three pooled independent experiments. **(D)** MIR99AHG mRNA expression by RT-qPCR from IL-4Rα$^{-/-}$ BMDMs stimulated with IL-4/IL-13 for 4 and 6 h. Data are representative of three pooled independent experiments. **(F, G)** RT-qPCR analysis of MIR99AHG kinetic mRNA expression in cytokine stimulated and Mtb HN878 infected BMDMs. Data are representative of three pooled independent experiments. **(H)** RT-qPCR analysis of MIR99AHG mRNA expression on whole lung from wild-type BALB/c mice infected with Mtb HN878 (100 CFU/mouse) for 11 and 21 days. Data are representative of three independent experiments. **(I)** RT-qPCR analysis of MIR99AHG kinetic expression in cytokine stimulated human MDMs. Data are representative of three pooled independent experiments. **(J)** RT-qPCR analysis of MIR99AHG kinetic expression in Mtb HN878 infected human MDMs. **(K, L)** Human MIR99AHG mRNA expression by RT-qPCR following IL-4/IL-13 and heat killed Mtb HN878 at 4 h poststimulation in PBMCs isolated from healthy and active TB patients. The fold change in gene expression was determined by RT-qPCR and was normalized to the housekeeping gene HPRT. Data are expressed as mean ± SD of triplicates. Data are representative of three independent experiments. *P* values represented as $*P<0.05$, $**P<0.01$, and $***P<0.001$; Two-way ANOVA **(C–F)** and Bonferroni *post hoc* test and Student's *t*-test **(F)**. ANOVA, analysis of variance; BMDMs, bone marrow-derived macrophages; CAGE, cap analysis of gene expression; MDMs, monocyte-derived macrophages; PBMCs, peripheral blood mononuclear cells; RT-qPCR, quantitative real-time polymerase chain reaction; SD, standard deviation; TB, tuberculosis.

MDMs was upregulated by IL-4/IL-13 stimulation and downregulated by Mtb HN878 infection (Fig. 1I, J). We restimulated PBMCs from healthy and active TB patients with IL-4/IL-13 and heat-killed Mtb HN878 for 4 h and observed reduced mRNA expression of MIR99AHG (Fig. 1K, L). Altogether, these data show that MIR99AHG expression varies according to the macrophage polarization state; in IL-4/IL-13 polarized macrophages MIR99AHG expression was induced, while the expression of MIR99AHG was downregulated following Mtb HN878 infection and in active TB patients.

To confirm whether other Mtb strains and other species of mycobacterium can regulate MIR99AHG expression, BMDMs were polarized with IL-4/IL-13 and then infected with the laboratory H37Rv, H37Ra strain, and *M. bovis* BCG to measure MIR99AHG mRNA expression by RT-qPCR (Supplementary Fig. S1A–C). Similarly, to Mtb HN878, H37Rv and H37Ra infection resulted in the downregulation of MIR99AHG mRNA expression at 4 h postinfection (Supplementary Fig. S1A, B). In contrast, *M. bovis* BCG infection resulted in the upregulation of MIR99AHG (Supplementary Fig. S1C).

MIR99AHG downregulation was also observed in BMDMs prestimulated with IL-4/IL-13 and infected with *L. mexicana* (Supplementary Fig. S1D) suggesting that MIR99AHG is downregulated by other intracellular pathogens that infect macrophages. To confirm whether other intracellular pathogens could reduce MIR99AHG expression, mice were infected with *L. monocytogenes* to determine MIR99AHG mRNA expression by RT-qPCR. Whole spleen and liver of mice infected *with L. monocytogenes* significantly displayed reduced mRNA expression of MIR99AHG at 2 days postinfection (Supplementary Fig. S1E, F).

Mtb HN878-induced suppression of MIR99AHG is mediated by NF-κB but not p38 signaling pathway, and MIR99AHG expression is differentially regulated by toll like receptor agonists

We used RT-qPCR to examine the kinetics of MIR99AHG expression in BMDMs exposed to toll like receptor (TLR) ligands, including CpG (TLR-9), lipopolysaccharide (LPS) (TLR-4), and Pam3CSK4 (TLR-2/1). The response of mRNA expression of MIR99AHG was significantly downregulated in BMDMs exposed to LPS and Pam3CSK4 in a time dependent manner but significantly upregulated in BMDM exposed CpG at 4 h poststimulation (Fig. 2A–C). Selective pharmacological inhibitors for NF-κB (Bay11–7082) and p38 (SB203580) were used to assess the functional relevance of these signaling pathways on regulating MIR99AHG expression. The p38 inhibitor (SB203580) did not restore the downregulation of MIR99AHG expression by Mtb HN878 infection (Fig. 2D). In contrast, the NF-κB inhibitor (Bay11–7082) restored the Mtb HN878-induced downregulation of MIR99AHG expression (Fig. 2D). Collectively, these results indicate that the NF-κB but not the p38 signaling pathway is responsible for the Mtb-mediated downregulation of MIR99AHG.

Knockdown of MIR99AHG by ASOs reduces intracellular Mtb growth, necrosis, and pro-inflammatory cytokines and increases early apoptosis in murine macrophages

To examine the functional role of MIR99AHG in regulating the intracellular growth of Mtb in murine macrophages, we

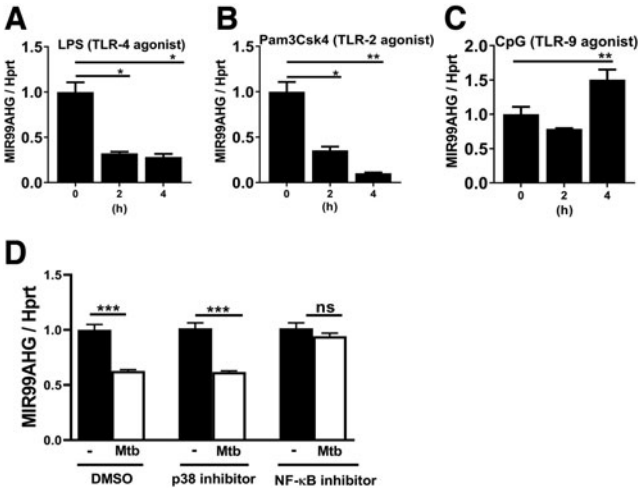

FIG. 2. MIR99AHG downregulation by Mtb in murine macrophages is mediated by the NF-κB but not the p38 signaling pathway, and MIR99AHG expression is differentially regulated by TLR agonists. **(A–C)** RT-qPCR of MIR99AHG mRNA expression in BMDMs stimulated with TLR-9 agonist CpG (500 nM), TLR-4 agonist LPS (100 ng/mL), and TLR-2 agonist Pam3Csk4 (100 ng/mL). Data are representative of three pooled independent experiments. **(D)** BMDMs were pretreated for 1 h with selective pharmacological inhibitors for NF-κB (Bay11–7082; 10 μM), p38 (SB203580; 5 μM) and infected with Mtb HN878 for 4 h. Expression of MIR99AHG mRNA was detected by RT-qPCR. Data are representative of three independent experiments. Data are expressed as mean ± SD of triplicates. *P* values are represented as $*P < 0.05$, $**P < 0.01$, and $***P < 0.001$, Student's *t*-test. LPS, lipopolysaccharide; NS, not significant; TLR, toll like receptor.

performed lncRNA loss-of-function experiments using LNA chemically engineered GapmeR ASOs. We first measured the knockdown efficiency of ASOs in M2 (IL-4/IL-13) polarized macrophages and identified a 92% reduction of MIR99AHG expression at 4 h post IL-4/IL-13 stimulation measured by RT-qPCR (Fig. 3A). We also identified a 73% reduction of MIR99AHG expression at 24 h post IL-4/IL-13 stimulation (Fig. 3A) and a 69% reduction at 4 h post Mtb HN878 infection (Fig. 3B). ASO treatment for MIR99AHG did not result in any macrophage cell toxicity during IL-4/IL-13 stimulation and Mtb HN878 infection as we identified stable cell viability measured by the CellTiter-Blue assay (Fig. 3C).

To examine the functional role of MIR99AHG during Mtb HN878 infection, we inhibited MIR99AHG using ASOs and analyzed its effect on the intracellular growth of Mtb in macrophages by CFU assays. Knockdown of MIR99AHG by ASOs significantly reduced the intracellular Mtb growth in IL-4/IL-13 stimulated macrophages at 72 h post Mtb HN878 infection (Fig. 3D) but did not change the phagocytic ability of macrophages to uptake Mtb at 4 h postinfection. This nonsignificant change in CFU at 4 h postinfection between the control and ASO-MIR99AHG treated macrophages is an important measure because it rules out impairment in the phagocytic uptake of Mtb by the macrophage.

Knockdown of MIR99AHG by ASOs led to an increased early apoptosis and reduced necrosis measured by Annexin V and 7AAD staining in IL-4/IL-13 stimulated BMDMs following Mtb HN878 infection, suggesting a possible

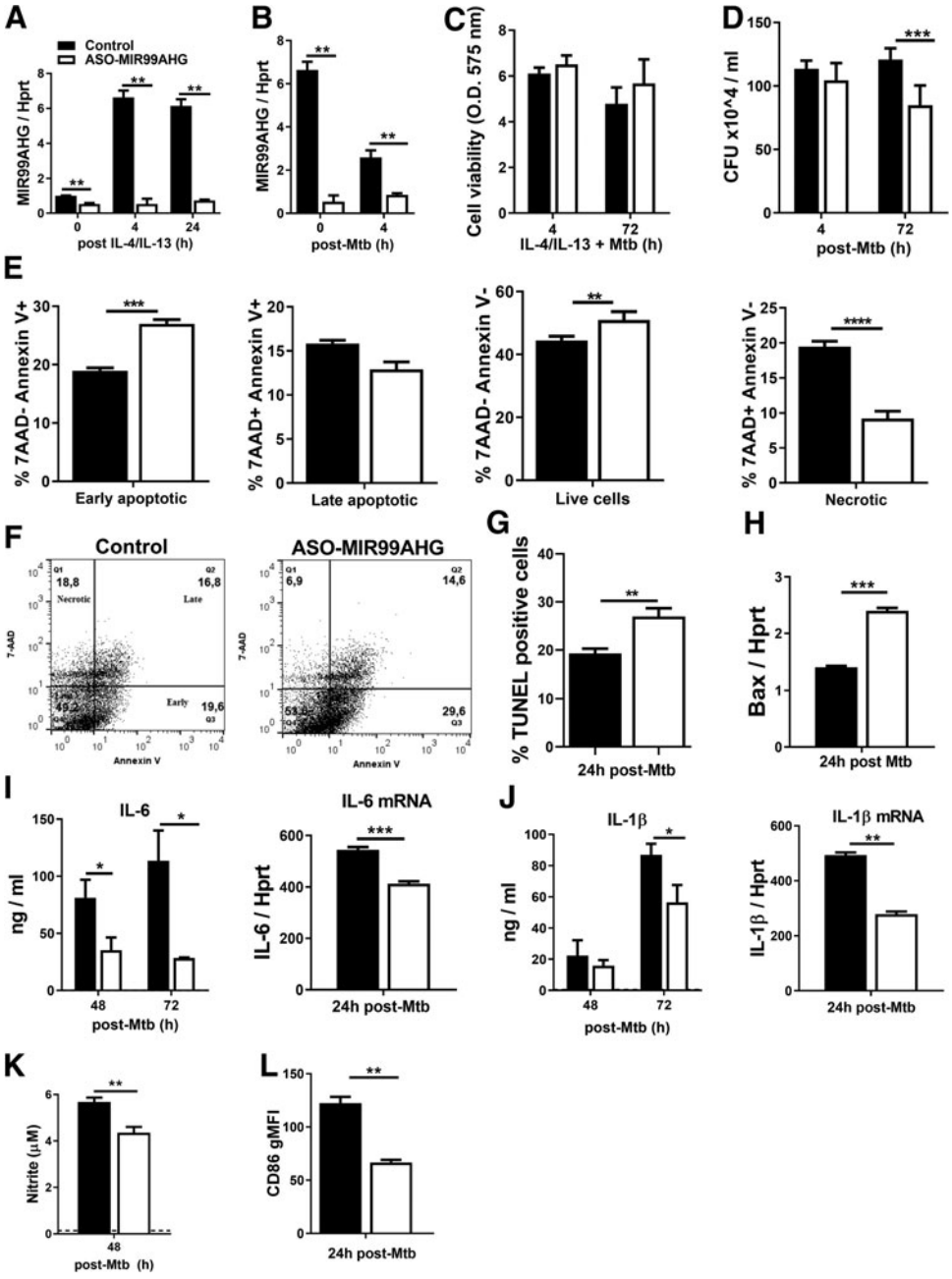

FIG. 3. Knockdown of MIR99AHG by ASOs reduces intracellular Mtb growth, necrosis, pro-inflammatory cytokines and increases early apoptosis in murine macrophages. BMDMs were ASO transfected with locked nucleic acid control and ASO-MIR99AHG, stimulated with IL-4/IL-13 for 4 h and infected with Mtb HN878. **(A)** MIR99AHG mRNA expression by RT-qPCR in ASO-treated BMDMs post IL-4/IL-13 stimulation **(B)** and post Mtb HN878 infection. Data are representative of three independent experiments. **(C)** Cell viability was measured in BMDMs at 4 and 72 h post Mtb HN878 infection by CellTiter Blue. Data are representative of three independent experiments. **(D)** BMDMs were ASO transfected with control and ASO-MIR99AHG, prestimulated with IL-4/IL-13 for 4 h, and infected with Mtb HN878. BMDMs were lysed at 4 h uptake and 72 h post-Mtb HN878 infection to measure mycobacterial growth by CFU counting. Data are representative of three pooled independent experiments. **(E–H)** BMDMs were ASOs treated with control and ASO-MIR99AHG for 48 h, then stimulated with IL-4/IL-13 for 4 h and infected with Mtb HN878 for 24 h to measure early apoptotic, late apoptotic, necrotic, and live cells with Annexin V and 7-AAD staining by flow cytometry. Data are representative of three independent experiments. **(F)** Representative flow dot plots by flow cytometry. **(G)** At 24 h post Mtb HN878 infection, BMDMs were labeled with the TUNEL reaction mixture and the percentages of TUNEL positive apoptotic cells analyzed by fluorescent microscopy. Data are representative of two independent experiments. **(H)** BMDMs were ASO transfected with control and ASO-MIR99AHG, prestimulated with IL-4/IL-13 for 4 h, infected with Mtb HN878, and RNA collected at 24 h post Mtb. Bax mRNA expression by RT-qPCR in BMDMs infected with Mtb HN878 at 24 h postinfection. Data are representative of three independent experiments. **(I, J)** Protein and mRNA cytokine levels of IL-6 and IL-1β measured by ELISA and RT-qPCR. Data are representative of three independent experiments. **(K, L)** Nitrite production measured by Griess reagent assay and CD86 gMFI by flow cytometry. Data are representative of three independent experiments. Data are expressed as mean ± SD of triplicates **(A, B, C, E, H, K, L)** and quadruplets **(D, I, J)**. *P* values represented as $*P < 0.05$, $**P < 0.01$, $***P < 0.001$, and $****P < 0.0001$; Student's *t*-test. ASO, antisense oligonucleotide; CFU, colony forming unit; ELISA, enzyme-linked immunosorbent assay; Mtb, *Mycobacterium tuberculosis*; TUNEL, terminal deoxynucleotidyl transferase dUTP nick-end labeling.

mechanism for the reduced intracellular Mtb growth (Fig. 3E, F and Supplementary Fig. S2B). Knockdown of MIR99AHG by ASOs led to increased apoptosis as measured by staining for DNA strand breakage using the TUNEL assay (Fig. 3G) at 24 h post Mtb infection. Using RT-qPCR, apoptosis was further confirmed at 24 h post Mtb HN878 infection by measuring the mRNA expression of Bax, a pro-apoptotic marker, which was significantly increased in ASO MIR99AHG treated BMDMs (Fig. 3H). We chose to measure early apoptosis and Bax at 24 h post Mtb infection as more than 80% of macrophages have phagocytosed mycobacteria at this time point.

To further characterize the functional role of MIR99AHG in modulating pro-inflammatory cytokine responses, we collected supernatant and RNA from ASO transfected BMDMs and performed ELISA and RT-qPCR. Protein and mRNA levels of IL-6 (Fig. 3I) and IL-1β (Fig. 3J) were significantly reduced in ASO MIR99AHG treated BMDMs compared to controls following IL-4/IL-13 stimulation and Mtb HN878 infection. We measured nitrite production by Griess reagent assay from ASO transfected BMDMs, stimulated with IL-4/IL-13 and infected with Mtb HN878. Knockdown of MIR99AHG by ASOs significantly reduced nitrite production compared to control in IL-4/IL-13 stimulated and Mtb HN878 infected macrophages (Fig. 3K). Furthermore, the silencing of MIR99AHG by ASOs significantly decreased CD86 gMFI, a known marker for classically activated macrophages (Fig. 3L). These data suggest that Mtb regulates inflammatory host responses by targeting MIR99AHG to promote intracellular growth in macrophages.

Knockdown of MIR99AHG by ASOs reduces intracellular Mtb growth, IL-6, and Bax in Mtb-infected human macrophages

To confirm the results observed in mouse macrophages, we examined the expression of MIR99AHG in MDMs. We used RT-qPCR to examine the kinetics of MIR99AHG expression on ASO transfected human MDMs prestimulated with IL-4/IL-13 and infected with Mtb HN878. The expression of human MIR99AHG was downregulated in IL-4/IL-13 polarized macrophages following Mtb HN878 infection (Fig. 4A). Human MDMs were viable following ASO treatment as confirmed by CellTiter-blue (Fig. 4B). Knockdown of MIR99AHG by ASOs significantly reduced Mtb intracellular growth in human MDMs (Fig. 4C). The mRNA levels of the pro-apoptotic marker Bax were significantly increased in MIR99AHG ASO treated human MDM at 24 h post Mtb HN878 infection (Fig. 4D). In IL-4/IL-13 stimulated and Mtb HN878 infected human MDMs, the knockdown of MIR99AHG by ASOs resulted in significantly reduced protein levels of IL-6 (Fig. 4E). These results demonstrate that MIR99AHG is targeted by Mtb to promote intracellular growth in human macrophages.

In vivo *ASO knockdown of MIR99AHG reduces mycobacterial burden in mice and pro-inflammatory responses in lung macrophages*

Targeting of noncoding RNAs to promote host innate defence is a promising strategy in the development of novel therapeutic interventions against TB [3,33]. To investigate whether the *in vitro* beneficial effects of MIR99AHG suppression in reducing intracellular Mtb growth and pro-inflammatory cytokines (Fig. 2) could be translated into an *in vivo* host-directed therapy (HDT), we used antisense LNA-modified GapmeR ASOs to inhibit MIR99AHG in a mouse Mtb infection model.

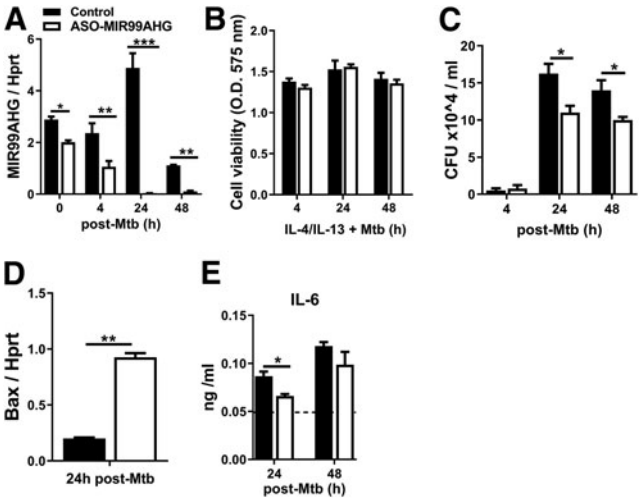

FIG. 4. Knockdown of MIR99AHG by ASOs reduces intracellular Mtb growth, IL-6, and Bax in Mtb-infected human macrophages. **(A)** MDMs were ASOs transfected with control and ASO-MIR99AHG, prestimulated with IL-4/IL-13 and infected with Mtb HN878. MIR99AHG mRNA expression by RT-qPCR in ASO-treated MDMs. Data are representative of three independent experiments. **(B)** Cell viability of ASO transfected human MDMs prestimulated with IL-4/IL-13 for 4 h and infected with Mtb HN878. Data are representative of three independent experiments. **(C)** MDMs were ASO transfected with control and ASO-MIR99AHG, prestimulated with IL-4/IL-13 for 4 h and infected with Mtb HN878. Cells were lysed at 4 h for uptake and 24 and 48 h post-Mtb HN878 infection to measure bacterial growth by CFU counting. Data are representative of three pooled independent experiments. **(D)** Bax mRNA expression by RT-qPCR in human MDMs infected with Mtb HN878. Data are representative of three independent experiments. **(E)** IL-6 production in human MDMs prestimulated with IL-/IL-13 for 4 h and infected with Mtb HN878 measured by ELISA. Data are representative of three independent experiments. Data are expressed as mean ± SD of triplicates. *P* values represented as $*P < 0.05$, $**P < 0.01$, and $***P < 0.001$, Student's *t*-test.

First, the mice were subcutaneously treated with ASOs for MIR99AHG or control (Antisense LNA GapmeR Negative control A) at 10 mg/kg for alternate days up to day 14. Mice were then infected with the hypervirulent clinical Mtb HN878 strain (100 CFU/mouse) intranasally for 21 days. RT-qPCR results showed that ASO treatment drastically suppressed MIR99AHG expression in lung tissues with a knockdown efficiency of 73% (Fig. 5A). Mice treated with MIR99AHG ASOs showed significantly reduced mycobacterial load in the lungs and in the spleen compared to the control mice (Fig. 5B, C). There was no difference in the Mtb uptake into the lungs measured by CFU assay at 1 day postinfection between the control mice and MIR99AHG ASO-treated mice (Fig. 5D).

At 3 weeks postinfection, there was reduced percentage of neutrophils (Neut) in the lungs in the ASO-MIR99AHG treated mice compared to the control mice (Fig. 5E). MPO assay validated reduced Neut influx into lungs in MIR99AHG ASO-treated mice (Fig. 5F). T cell recruitment, measured by CD3 staining, was significantly reduced in MIR99AHG ASO-treated mice

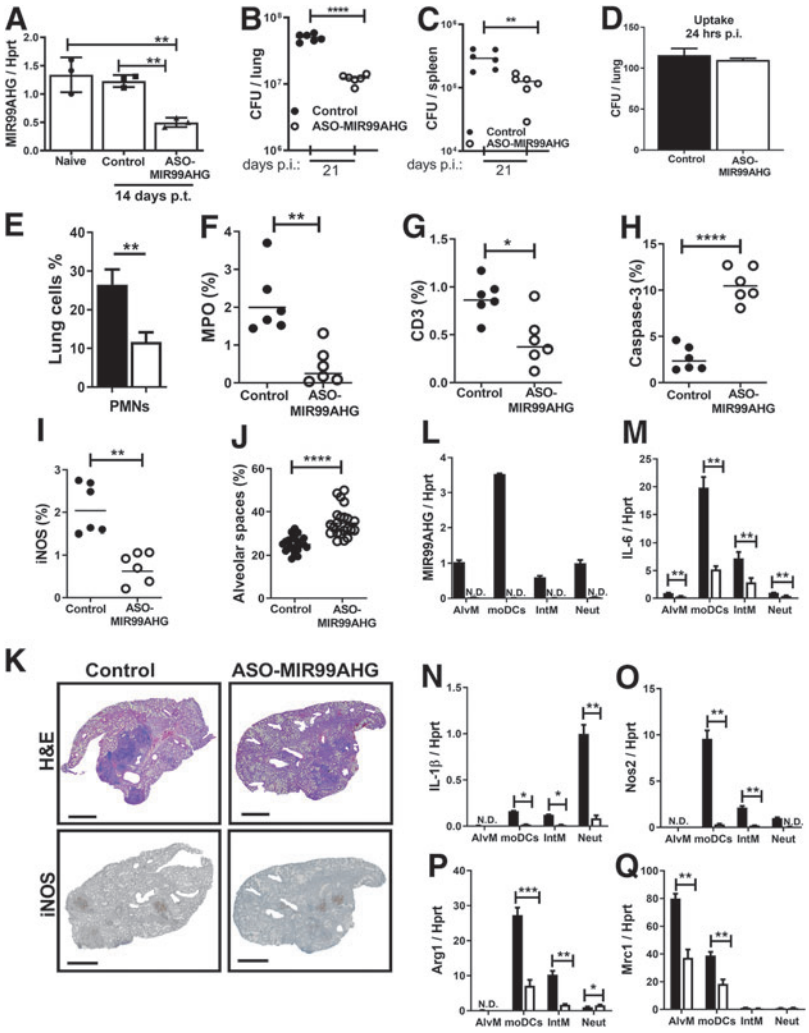

FIG. 5. *In vivo* ASO knockdown of MIR99AHG reduces mycobacterial burden in mice and pro-inflammatory responses in lung macrophages. BALB/c mice ($n = 6$/mice/group) were ASO treated with 10 mg/kg locked nucleic acid control and ASO-MIR99AHG. **(A)** MIR99AHG mRNA expression by RT-qPCR at 14 days post ASO treatment. **(B, C)** Mycobacterial burden of Mtb HN878-infected mice is shown with indicated CFU in lung and spleen at 3 weeks postinfection. **(D)** Mtb HN878 infected mice were sacrificed at 24 h postinfection to determine the CFU lung uptake ($n = 3$ mice/group). **(E)** Percentage of lung neutrophils at 3 weeks postinfection quantified by flow cytometry. **(F–I)** The percentage of positive MPO, CD3, Caspase-3, and iNOS staining was quantified from two deep cut lung sections per mice at 3 weeks post Mtb HN878 infection (30 μm apart). **(J)** Alveolar spaces at 3 weeks postinfection were quantified from four deep cut H&E lung sections per mice (30 μm apart). **(K)** Representative histopathology sections (2× magnification) at 3 weeks postinfection for H&E and iNOS (scale bar = 1,000 μm). **(L–Q)** At 3 weeks postinfection, $CD64^+CD11c^+SiglecF^+$ AlvM, $CD11b^+CD11c^+CD64^+$ (moDCs), $CD64^+CD11b^+CD11c^-SiglecF^-$ IntM, and $CD11b^+LY6G^+$ neutrophils were sorted by flow cytometry to determine lung mRNA expression of MIR99AHG, *IL6, IL1b, Nos2,* Arg1, and Mrc1 by RT-qPCR. Data are expressed as mean ± SD. *P* values represented as $^*P < 0.05$, $^{**}P < 0.01$, and $^{****}P < 0.0001$; Student's *t*-test. AlvM, alveolar macrophages; iNOS, inducible nitric oxide synthase; IntM, interstitial recruited macrophage, MPO, myeloperoxidase; N.D., not detected.

(Fig. 5G). Caspase-3, a marker for apoptosis, was significantly increased in MIR99AHG ASO-treated mice compared to the control group (Fig. 5H). Staining of lung sections with iNOS, the enzyme responsible for producing the antimycobacterial effector molecule NO, was significantly reduced in MIR99AHG ASO-treated mice compared to the control group (Fig. 5I, K) suggesting that the observed antimycobacterial effector functions were independent of iNOS. Alveolar spaces measured on H&E lung sections were significantly increased in MIR99AHG ASO-treated mice compared to the control mice at 3 weeks post Mtb HN878 infection, suggesting reduced pulmonary lesion sizes following MIR99AHG inhibition (Fig. 5J, K).

To better define inflammatory responses in the lungs following MIR99AHG ASO treatment, myeloid cell populations were sorted with flow cytometry to measure mRNA expression by RT-qPCR at 3 weeks post Mtb HN878 infection. MIR99AHG expression was expressed in alveolar macrophages (AlvM), monocyte-derived dendritic cells (moDCs), interstitial recruited macrophage (IntM), and Neut from Mtb HN878 infected control mice but absent in MIR99AHG ASO-treated mice (Fig. 5L).

Notably, MIR99AHG ASO treatment displayed significantly reduced levels of pro-inflammatory cytokines, such as

il6 and *il1b*, compared to controls mainly in moDCs, IntM, and Neut cell populations (Fig. 5M, N). In addition, nitric oxide synthase (NOS2) and Arg1 and Mrc1 mRNA expression were significantly reduced in moDCs, IntM, and AlvM from Mtb HN878 infected MIR99AHG ASO-treated mice (Fig. 5O–Q). T lymphocyte population in the lungs was not affected by the knockdown of MIR99AHG except for increased percentage of $CD4^+$ $T_{effector}$ cells (Supplementary Figs. S2A and S3A–D). Taken together, these results suggest that MIR99AHG contributes to mycobacterial growth, increases pulmonary histopathology, and enhances pro-inflammatory responses in lung macrophages.

MIR99AHG is translocated from the cytoplasm to the nucleus following IL-4/IL-13 stimulation and interacts with hnRNPA2/B1

To understand how MIR99AHG regulates inflammatory responses in macrophages, we examined its location by performing subcellular fractionation and analyzed the

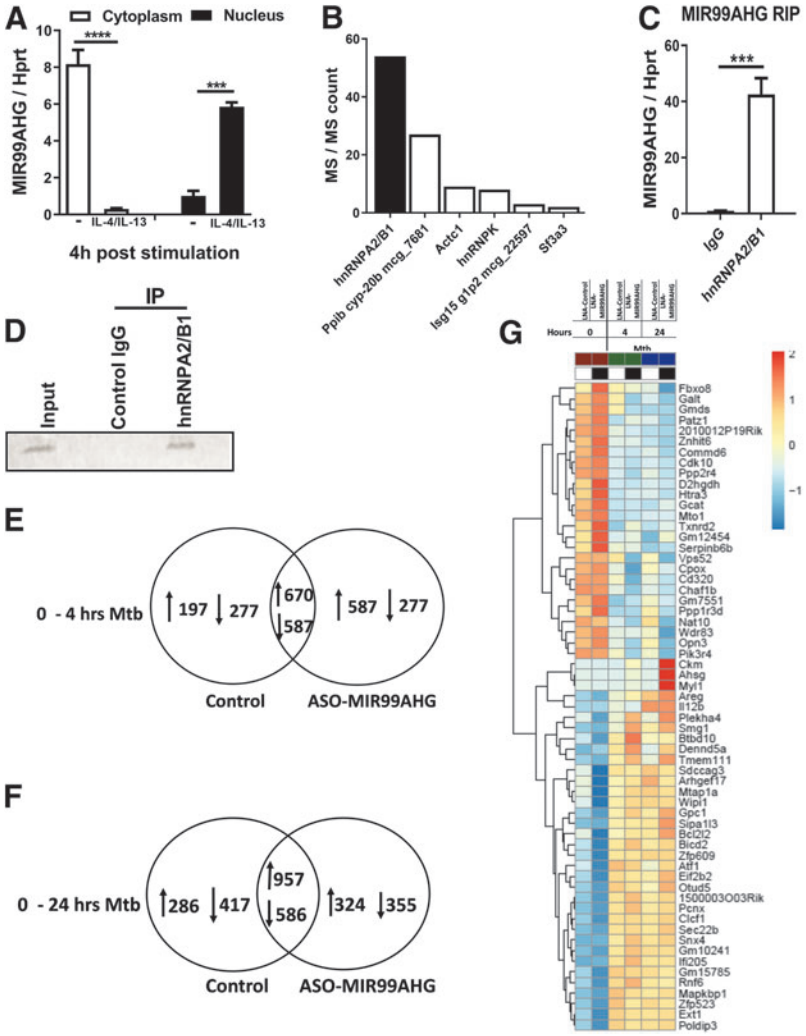

FIG. 6. MIR99AHG is translocated from the cytoplasm to the nucleus following IL-4/IL-13 stimulation and interacts with hnRNPA2/B1 in murine macrophages. **(A)** RT-qPCR analysis of RNAs purified from nuclear and cytoplasm compartments in BMDMs stimulated with IL-4/IL-13 for 4h. Data are representative of three independent experiments. **(B)** The six most enriched proteins associated with MIR99AHG identified by affinity purification and mass spectrometry in ASO treated BMDMs prestimulated with IL-4/IL-13 for 4 h and infected with Mtb HN878 for 24 h. Data are representative of three independent experiments. **(C)** hnRNPA2/B1 RIP followed by mRNA expression of MIR99AHG by RT-qPCR in anti-hnRNPA2/B1 antibody or control IgG immunoprecipitates from nuclear lysates of macrophages prestimulated with IL-4/IL-13 for 4 h and infected with Mtb HN878 for 24 h. **(D)** Western blot of hnRNPA2/B1 in Input, anti-hnRNPA2/B1 antibody, and control IgG immunoprecipitates from nuclear lysates of macrophages prestimulated with IL-4/IL-13 for 4 h and infected with Mtb HN878 for 24 h. **(E–G)** BMDMs were ASO transfected with locked nucleic acid control and ASO-MIR99AHG for 48 h and infected with Mtb HN878 for 4 and 24 h. **(E, F)** Venn diagrams displaying up- and downregulated genes between control ASO-MIR99AHG at 4 and 24 h post Mtb infection. Data are representative of three independent experiments. **(G)** Heatmap representative of genes commonly upregulated and downregulated at 4 and 24 h post Mtb infection. Each row (gene) was centered on the mean expression value across all samples. Data are representative of three independent experiments. Data shown are mean of three replicates. Data are expressed as mean ± SD **(A, C)** of triplicates. *P* values represented as $***P < 0.001$ and $****P < 0.0001$, Student's *t*-test. RIP, RNA immunoprecipitation.

expression of MIR99AHG by RT-qPCR. This analysis revealed that MIR99AHG was predominantly found in the cytoplasm in unstimulated BMDMs but upon IL-4/IL-13 stimulation MIR99AHG translocated to the nucleus (Fig. 6A) suggesting that MIR99AHG may exert its biological functions in the nucleus in M2 (IL-4/IL-13) polarized macrophages.

To identify MIR99AHG binding proteins, we performed RNA pulldown assay *in vitro* by incubating transcribed biotinylated MIR99AHG and its antisense control RNA with nuclear extracts from IL-4/IL-13 stimulated and Mtb HN878 infected BMDMs. The associated proteins were pulled down and analyzed by mass spectrometry. We identified the six most enriched MIR99AHG-binding proteins based on the number of peptides specifically associated with MIR99AHG (Fig. 6B). Among the six genes identified, hnRNPA2/B1 had the highest number of peptides associated with MIR99AHG (Fig. 6B). To confirm hnRNPA2/B1-MIR99AHG interaction, we performed RNA immunoprecipitation of endogenous hnRNPA2/B1 nuclear extracts of BMDMs stimulated with IL-4/IL-13 and infected with Mtb HN878 followed by RT-qPCR analysis and Western blot (Fig. 6C, D). These data show that MIR99AHG is translocated to the nucleus upon IL-4/IL-13 stimulation and interacts with hnRNPA2/B1 in macrophages.

To assess the impact of MIR99AHG knockdown on gene expression in macrophages, we performed RNA-seq in MIR99AHG knockdown BMDMs infected with Mtb HN878 for 4 and 24 h (Fig. 6E, F). BMDMs were transfected with control and ASO-MIR99AHG for 48 h before Mtb infection. We regarded this time point as 0 h. BMDMs were then infected with Mtb HN878 for 4 and 24 h. We compared up- and downregulated genes in control treated and ASO-MIR99AHG treated BMDMs at 4 and 24 h post Mtb (Fig. 6E, F). The heatmap shows 61 genes that are constantly up- and downregulated at 4 and 24 h post Mtb infection (Fig. 6G). The most downregulated genes in MIR99AHG versus control at 24 h post Mtb infection include Fbxo8, Galt, Gmds, Patz1, and Znhit6 (Fig. 6G). The most upregulated genes in MIR99AHG vs control at 24 h post Mtb infection include Ckm, Ahsg, Myl1, il12b, and Areg (Fig. 6G). Some of the upregulated genes that were significantly enriched were related to regulation of inflammatory responses and activation of innate immune response (Fig. 6G).

Discussion

The main purpose of host-directed therapies (HDTs) is to eliminate Mtb with minimal damage to the host [34]. HDTs include different groups of compounds, such as cytokines and repurposed drugs, that target biologically and clinically relevant checkpoints in anti-Mtb-directed host response pathways [34]. Adjunctive HDTs have the potential to shorten TB treatment duration, prevent antibiotic resistance, and reduce lung injury by promoting autophagy, antimicrobials, and other macrophage effector mechanisms [35]. Corticosteroids have been used as adjunctive therapy for many inflammatory and disease states [36,37]. The rationale for using corticosteroids in active TB disease involves modulation of inflammatory and apoptotic gene transcription pathways [38]. Corticosteroids as immunoadjuvants to standard TB treatments have proven to be useful in several studies, including treatment of HIV/TB coinfection [39–42].

The first therapeutic nucleic acid, DNA-based oligonucleotide, approved by the FDA was Fomivirsen [43]. Recently, the first RNA-based ASO was approved by the FDA [44]. This treatment approach promises to be a growing field as many biopharmaceutical companies are developing RNA interference (RNAi)-based and RNA-based ASO therapies [45]. The potential of using lncRNAs and miRNAs as adjunctive HDT is a topic that is gaining momentum especially in the context of treating infectious diseases. A handful of miRNA-targeting drugs have entered into clinical trials targeting different diseases [45].

M2 (IL-4/IL-13) polarized macrophages are immune modulators that secrete ornithine and mediate Th2-associated effector functions [46]. Mtb neutralizes microbicidal effectors to promote M2 (IL-4/IL-13) polarization state to promote persistence and survival in macrophages [46]. An effective immune defence against intracellular pathogens is dependent on a wide transcriptional program in macrophages and other immune cells [47]. While the role of miRNAs in the regulation host inflammatory responses has been well studied [48], the role of lncRNAs in macrophages and during Mtb infection is still poorly understood.

In this study, we demonstrate that the long intergenic noncoding RNA, MIR99AHG, is highly upregulated in M2 (IL-4/IL-13) polarized macrophages. We analyzed the expression of MIR99AHG in murine macrophages infected with either hypervirulent Mtb HN878, virulent Mtb H37Rv, or avirulent Mtb H37Ra and *M. bovis* BCG strains. MIR99AHG was downregulated by Mtb HN878, Mtb H37Rv, and Mtb H37Ra infection but upregulated in *M. bovis* BCG infected macrophages. Similarly, lncRNAs, HOTAIR, were downregulated by Mtb H37Rv but upregulated by Mtb H37Ra [49].

Using antisense therapy (ASOs), we gained insights into the biological functions of MIR99AHG at both cellular level and organismal level. Knockdown of MIR99AHG by ASOs reduced intracellular Mtb growth in mouse and human macrophages, induced apoptosis, and inhibited necrosis. Knockdown of MIR99AHG by ASOs reduced pro-inflammatory cytokines such as IL-6 and IL-1β. *In vivo* inhibition of MIR99AHG by ASOs reduced mycobacterial burden in the lung and spleen and reduced pro-inflammatory responses in lung macrophages. We show that MIR99AHG interacts with hnRNPA2/B1. We further demonstrate that MIR99AHG is translocated to the nucleus following IL-4/IL-13 stimulation.

MIR99AHG was previously identified and referred to as MONC [50]. MIR99AHG was reported to be spliced into a 710-nucleotide lincRNA, where intron 6 of MONC produces three miRNAs *MIR99A*, *LET7C*, and *MIR125B2* [50]. The knockdown of MIR99AHG by shRNAs in acute megakaryoblastic leukemia (AMKL) cell lines reduced leukemic growth [50]. Similar to our study, upon MIR99AHG knockdown by ASOs, apoptosis was increased in AMKL cell lines [50]. Furthermore, MONC was predominantly located in the nucleus [50]. In a recently published article MIR99-AHG was downregulated in lung adenocarcinoma tissues [51]. Knockdown of MIR99AHG suppressed the proliferation and metastasis and increased autophagy *in vitro* and *in vivo* in H1299 or A549 cells [51].

IL-4 signals through two different receptor complexes, type I receptor (IL-4Rα/cγ chain) and type II receptor (IL-13Rα1) [52,53]. Since MIR99AHG is upregulated by IL-4/IL-13, we examined its expression in IL-4Rα$^{-/-}$ BMDMs and

in lung homogenate of naive and Mtb HN878 infected mice. We observed that MIR99AHG expression was mediated by the IL-4Rα signaling pathway in M2 (IL-4/IL-13) polarized macrophages (Supplementary Fig. S1). Interestingly, we observed high MIR99AHG expression in lung homogenates of naive, noninfected mice (Fig. 1H). This high MIR99AHG expression could potentially be explained by the high levels of IL-4 detected in lungs of naive BALB/c mice [54].

Apoptosis is an important innate host defence mechanism to control mycobacterial growth within macrophages [55]. It has been reported that virulent strains of Mtb inhibit apoptosis [56], while avirulent Mtb strains induce apoptosis in macrophages resulting in the inhibition of mycobacterial growth [57]. Furthermore, virulent Mtb infection causes necrosis in macrophages that allows mycobacterial dissemination [56]. Mtb has been shown to be able to survive in necrotic macrophages before escaping [58]. Corticosteroids which have been used as HDT were shown to inhibit the necrotic cell death of Mtb infected cells through the dephosphorylation of p38 MAPK [59]. Bax is a known proapoptotic marker, and this is supported by many previous studies who have measured the expression of Bax as a proapoptotic marker [60–65]. From our findings we show that the knockdown of MIR99AHG by ASOs increases apoptosis but reduces necrosis in Mtb HN878 infected macrophages.

The secretion of pro-inflammatory cytokines is crucially important in the protection of the host against Mtb infection. To control mycobacterial replication, cytokines such as IFNγ, TNFα, IL-6, and IL-1β are required for an effective host immune response against Mtb [66]. We examined whether knocking down of MIR99AHG would modulate proinflammatory cytokine production in macrophages. Knockdown of MIR99AHG by ASOs significantly reduced the production of IL-6 and IL-1β in M2 (IL-4/IL-13) polarized and Mtb HN878 infected macrophages suggesting that MIR99AHG may be a positive regulator of pro-inflammatory cytokine responses. A number of lncRNAs have been reported to regulate host inflammation or act as ''brakes'' in controlling excessive inflammation [14,16,18,67]. Our results suggest that MIR99AHG plays an immunomodulatory role as a potential regulator of macrophage polarization and inflammation promoting Mtb growth and persistence in macrophages.

The role of lncRNAs in cancer has been well studied; however, there is limited data available on characterized lncRNAs in a TB disease model. Recent studies have shown strong evidence on the role of lncRNAs in the modulation of innate and adaptive immune response [14,16,18,]. Findings from animal models, using systemic administration of ASOs, serve as a translational proof of concept for therapeutic interventions targeting lncRNAs [68]. In this study, we provide evidence for MIR99AHG modulating host immunity to Mtb infection. We explored the role of MIR99AHG in a loss of function approach using ASO therapy *in vivo*. Mice treated with MIR99AHG ASOs were more protected against TB disease exhibiting reduced lung inflammation.

In histological lung sections, Caspase-3 staining was significantly increased in the MIR99AHG ASO treated group suggesting increased apoptosis. Moreover, ASO treated murine macrophages displayed enhanced apoptosis and increased Bax Mrna expression following Mtb HN878 infection further supporting a possible mechanism for the observed reduced mycobacterial growth. NOS2 mRNA expression in lung macrophages was significantly reduced in ASO-MIR99AHG treated mice suggesting that the reduced mycobacterial burden was independent of NOS2 effector functions. Nitric oxide has been identified to be a key player in controlling Mtb infection [69]. We show for the first time that treatment with MIR99AHG ASOs significantly reduced the pathogenesis of Mtb HN878 infection, suggesting that MIR99AHG could be repurposed for host-directed therapy against TB.

The engagement of TLRs elicits signaling pathways that activate inflammatory genes, and many long noncoding RNAs have been shown to be induced by TLRs [14,16,18,67]. Long noncoding RNAs have emerged as new regulators of inflammatory mediators in the immune system. In this study we show that the response of mRNA expression of MIR99AHG was significantly upregulated in BMDMs exposed to CpG (TLR-9) at 4 h poststimulation suggesting that MIR99AHG upregulation is signaled through TLR-9 and MIR99AHG downregulation is signaled through TLR-2/4 (Fig. 2A–C).

Similarly, THRIL (TNF-α hnRNPL Related Immunoregulatory Long noncoding RNA) was shown to be downregulated following TLR-2 stimulation in THP-1 cells [17]. In contrast to THRIL, lincRNA-Cox2 was highly upregulated by TLR-2 and TLR-4 [16] in BMDMs. NKILA is another lncRNA upregulated by TLR-4 stimulation in MDA-MB-231 in breast cancer cells [70]. There have been no published lncRNAs reported to be upregulated or downregulated by TLR-9. Many functions of lncRNAs are mediated through control of TLR signaling, and altered expression and activities of lncRNAs have been implicated in the pathogenesis of infectious and inflammatory diseases [71].

Our study demonstrated that MIR99AHG interacted with hnRNPA2/B1. Interestingly, hnRNPA2/B1 has been shown to interact with *lincRNA-COX2* to regulate immune response genes during inflammatory responses [16]. Macrophages lacking the expression of hnRNPA2/B1 by shRNA resulted in enhanced levels of *Ccl5, Trl7, Il6, Il1b, Stat1, and IκB* following LPS and Pam3Csk4 stimulation [16]. In our study we showed that knockdown of MIR99AHG by ASOs reduced *Il6, Il1b,* and *Nos2* mRNA expression. The hnRNP family acts as mediators of lncRNA-induced transcriptional gene repression [72,73]. The interaction of lncRNA-p53 with its protein binding partner hnRNP-K is essential for the genomic localization of hnRNP-K at repressed genes and the regulation of p53 mediated apoptosis [73]. hnRNPs are important functional partners for many additional lncRNAs. These include *lincRNA-EPS* which interacts with hnRNPL [14]. *lincRNA-p21* [73] and *Xist* [72] have been identified as binding partners of hnRNPK and hnRNPU, respectively.

hnRNPs are well known to be involved in mRNA biogenesis. In addition, the role of hnRNPA2/B1 in transcriptional regulation of gene expression is emerging. For example, hnRNPA2/B1 that interacts with small activating dsRNA to induce transcriptional activation is required [74]. Moreover, hnRNPA2/B1 is required for smooth muscle cell (SMC) differentiation gene expression. hnRNPA2/B1 promotes neural crest cell migration [75]. The identification of hnRNPA2/B1 as a functional binding partner of MIR99AHG adds further support to the role of hnRNPs in transcriptional

regulation. The MIR99AHG-hnRNPA2/B1 interaction observed in this article is of importance; further experiments need to be performed to understand the mechanism and significance of this interaction on target genes to fully substantiate this interaction. In addition, further work can be performed such as mapping of the binding domains of the interacting partners and mutational analysis to understand the consequences of abrogating the interaction.

Our RT-qPCR results on purified RNA from the nucleus and cytoplasm compartments showed a nuclear localization of MIR99AHG upon IL-4/IL-13 stimulation. It is most likely that lncRNAs play an important role in the organization of nuclear domains [76]. In the nucleus, lncRNAs can act in *cis* or *trans*, for example, *Morrbid* interacts with PRC2 to repress transcription of the neighboring gene, Bim (*Bcl2l11*) [77]. A lncRNA can interact with its protein partner as a guide (lincRNA:hnRNPL) [14], scaffold (RMRP interaction with DDX5 and RORγt) [78], or decoy molecule (Lethe:NF-κB p65) [79] to mediate its molecular functions. Cellular localization of lncRNAs can help with studies involving functions and mechanisms of action. Further studies in identifying the exact subnuclear areas and DNA target sequences of MIR99AHG still need to be performed.

In conclusion, this study characterizes, for the first time, the functional role of MIR99AHG during Mtb HN878 infection. MIR99AHG plays an important role in the regulation of inflammatory genes and promotes Mtb growth in macrophages. In Mtb HN878 infected mice and macrophages, MIR99AHG promotes the intracellular survival of Mtb possibly through favoring macrophage necrosis. MIR99AHG, as adjunct to existing antibiotics, could potentially become a possible target for host-directed drug therapy for TB.

Acknowledgments

The authors acknowledge Dr. Paulin Essone, Dr. Berenice Maria Martinez-Salazar, Dr. Laurianne Davignon, Dr. Jermaine Khumalo, Dr. Takahiro Suzuki, and Ms Munadia Ansarie for their assistance. The authors also thank UCT Animal Unit for maintaining mice.

Disclaimer

The content is solely the responsibility of the authors and does not necessarily represent the official views of the National Institutes of Health. For the purpose of open access, the author has applied a CC BY public copyright licence to any Author Accepted Manuscript version arising from this submission.

Author Disclosure Statement

No competing financial interests exist.

Funding Information

This work was supported by the Department of Science and Technology (DST)/South African National Research Foundation (NRF) Innovation Doctoral Scholarship awarded to L.G.; DST/NRF postdoctoral innovation fellowship awarded to O.T.; the research grant for the Special Coordination Funds for Promoting Science and Technology from the Ministry of Education, Culture, Sports, Science and Technology (MEXT) awarded to H.S.; the grants from NRF/DST-South African Research Chair Initiative (SARCHi), South African Medical Research Council (SAMRC) and International Centre for Genetic Engineering and Biotechnology (ICGEB) awarded to F.B.

The Global Health Innovative Technology grant was awarded to F.B. and H.S. The NRF Competitive Programme for Unrated Researchers (CSUR) was awarded to R.G. The DST/NRF BRICS Multilateral Joint Science and Technology Research Collaboration grant (No. 110482) was awarded to R.G. The National Health Laboratory Service (NHLS) Research Trust and the NHLS (GRANT004–94836) were awarded to R.G. Research reported in this publication was supported by the National Institute of Allergy and Infectious Diseases of the National Institutes of Health under Award No. R01AI160501. This research was funded in whole, or in part, by the Wellcome Trust [203135/Z/16/Z]. K.D. is supported by the South African MRC (RAF-EMU-02-2017) and the EDCTP (TMA-2015SF-1043 and TMA- 1051-TESAII).

Supplementary Material

Supplementary Figure S1
Supplementary Figure S2
Supplementary Figure S3
Supplementary Figure S4

References

1. WHO. (2019). Global Tuberculosis Report. WHO Press.
2. Flynn JL and J Chan. (2001). Immunology of tuberculosis. Annu Rev Immunol 19:93–129.
3. Guler R and F Brombacher. (2015). Host-directed drug therapy for tuberculosis. Nat Chem Biol 11:748–751.
4. Fitzgerald KA and DR Caffrey. (2014). Long noncoding RNAs in innate and adaptive immunity. Curr Opin Immunol 26:140–146.
5. Consortium EP, E Birney, JA Stamatoyannopoulos, A Dutta, R Guigo, TR Gingeras, EH Margulies, Z Weng, M Snyder *et al.* (2007). Identification and analysis of functional elements in 1% of the human genome by the ENCODE pilot project. Nature 447:799–816.
6. Derrien T, R Johnson, G Bussotti, A Tanzer, S Djebali, H Tilgner, G Guernec, D Martin, A Merkel *et al.* (2012). The GENCODE v7 catalog of human long noncoding RNAs: analysis of their gene structure, evolution, and expression. Genome Res 22:1775–1789.
7. Guttman M and JL Rinn. (2012). Modular regulatory principles of large non-coding RNAs. Nature 482:339–346.
8. Gil N and I Ulitsky. (2020). Regulation of gene expression by cis-acting long non-coding RNAs. Nat Rev Genet 21: 102–117.
9. Lewandowski JP, JC Lee, T Hwang, H Sunwoo, JM Goldstein, AF Groff, NP Chang, W Mallard, A Williams *et al.* (2019). The Firre locus produces a trans-acting RNA molecule that functions in hematopoiesis. Nat Commun 10: 5137.
10. Yan P, S Luo, JY Lu and X Shen. (2017). Cis- and trans-acting lncRNAs in pluripotency and reprogramming. Curr Opin Genet Dev 46:170–178.
11. Atianand MK, DR Caffrey and KA Fitzgerald. (2017). Immunobiology of long noncoding RNAs. Annu Rev Immunol 35:177–198.

12. Denisenko E, D Ho, O Tamgue, M Ozturk, H Suzuki, F Brombacher, R Guler and S Schmeier. (2016). IRNdb: the database of immunologically relevant non-coding RNAs. Database (Oxford) 2016:baw138.
13. Elling R, J Chan and KA Fitzgerald. (2016). Emerging role of long noncoding RNAs as regulators of innate immune cell development and inflammatory gene expression. Eur J Immunol 46:504–512.
14. Atianand MK, W Hu, AT Satpathy, Y Shen, EP Ricci, JR Alvarez-Dominguez, A Bhatta, SA Schattgen, JD McGowan *et al.* (2016). A long noncoding RNA lincRNA-EPS acts as a transcriptional brake to restrain inflammation. Cell 165:1672–1685.
15. Ramilowski JA, CW Yip, S Agrawal, JC Chang, Y Ciani, IV Kulakovskiy, M Mendez, JLC Ooi, JF Ouyang *et al.* (2020). Functional annotation of human long noncoding RNAs via molecular phenotyping. Genome Res 30:1060–1072.
16. Carpenter S, D Aiello, MK Atianand, EP Ricci, P Gandhi, LL Hall, M Byron, B Monks, M Henry-Bezy *et al.* (2013). A long noncoding RNA mediates both activation and repression of immune response genes. Science 341: 789–792.
17. Li Z, TC Chao, KY Chang, N Lin, VS Patil, C Shimizu, SR Head, JC Burns and TM Rana. (2014). The long noncoding RNA THRIL regulates TNFalpha expression through its interaction with hnRNPL. Proc Natl Acad Sci U S A 111: 1002–1007.
18. Du M, L Yuan, X Tan, D Huang, X Wang, Z Zheng, X Mao, X Li, L Yang *et al.* (2017). The LPS-inducible lncRNA Mirt2 is a negative regulator of inflammation. Nat Commun 8:2049.
19. Castellanos-Rubio A, N Fernandez-Jimenez, R Kratchmarov, X Luo, G Bhagat, PH Green, R Schneider, M Kiledjian, JR Bilbao and S Ghosh. (2016). A long noncoding RNA associated with susceptibility to celiac disease. Science 352:91–95.
20. Li M, J Cui, W Niu, J Huang, T Feng, B Sun and H Yao. (2019). Long non-coding PCED1B-AS1 regulates macrophage apoptosis and autophagy by sponging miR-155 in active tuberculosis. Biochem Biophys Res Commun 509: 803–809.
21. Pawar K, C Hanisch, SE Palma Vera, R Einspanier and S Sharbati. (2016). Down regulated lncRNA MEG3 eliminates mycobacteria in macrophages via autophagy. Sci Rep 6:19416.
22. Wang Y, H Zhong, X Xie, CY Chen, D Huang, L Shen, H Zhang, ZW Chen and G Zeng. (2015). Long noncoding RNA derived from CD244 signaling epigenetically controls CD8+ T-cell immune responses in tuberculosis infection. Proc Natl Acad Sci U S A 112:E3883–E3892.
23. Kundu M and J Basu. (2021). The role of microRNAs and long non-coding RNAs in the regulation of the immune response to *Mycobacterium tuberculosis* infection. Front Immunol 12:687962.
24. Huang S, Z Huang, Q Luo and C Qing. (2018). The expression of lncRNA NEAT1 in human tuberculosis and its antituberculosis effect. Biomed Res Int 2018:9529072.
25. Li D, C Gao, L Zhao and Y Zhang. (2020). Inflammatory response is modulated by lincRNACox2 via the NFkappaB pathway in macrophages infected by *Mycobacterium tuberculosis*. Mol Med Rep 21:2513–2521.
26. Yang X, J Yang, J Wang, Q Wen, H Wang, J He, S Hu, W He, X Du *et al.* (2016). Microarray analysis of long noncoding RNA and mRNA expression profiles in human macrophages infected with *Mycobacterium tuberculosis*. Sci Rep 6:38963.
27. Heyer EE, H Ozadam, EP Ricci, C Cenik and MJ Moore. (2015). An optimized kit-free method for making strand-specific deep sequencing libraries from RNA fragments. Nucleic Acids Res 43:e2.
28. Guler R, SP Parihar, S Savvi, E Logan, A Schwegmann, S Roy, NE Nieuwenhuizen, M Ozturk, S Schmeier *et al.* (2015). IL-4Ralpha-dependent alternative activation of macrophages is not decisive for *Mycobacterium tuberculosis* pathology and bacterial burden in mice. PLoS One 10: e0121070.
29. Denisenko E, R Guler, MM Mhlanga, H Suzuki, F Brombacher and S Schmeier. (2017). Genome-wide profiling of transcribed enhancers during macrophage activation. Epigenetics Chromatin 10:50.
30. Roy S, S Schmeier, E Arner, T Alam, S P Parihar, M Ozturk, O Tamgue, H Kawaji, M J de Hoon *et al.* (2015). Redefining the transcriptional regulatory dynamics of classically and alternatively activated macrophages by deepCAGE transcriptomics. Nucleic Acids Res 43:6969–6982.
31. Denisenko E, R Guler, M Mhlanga, H Suzuki, F Brombacher and S Schmeier. (2019). Transcriptionally induced enhancers in the macrophage immune response to *Mycobacterium tuberculosis* infection. BMC Genomics 20:71.
32. Roy S, S Schmeier, B Kaczkowski, E Arner, T Alam, M Ozturk, O Tamgue, S P Parihar, H Kawaji *et al.* (2018). Transcriptional landscape of *Mycobacterium tuberculosis* infection in macrophages. Sci Rep 8:6758.
33. Man DK, MY Chow, L Casettari, M Gonzalez-Juarrero and JK Lam. (2016). Potential and development of inhaled RNAi therapeutics for the treatment of pulmonary tuberculosis. Adv Drug Deliv Rev 102:21–32.
34. Hawn TR, AI Matheson, SN Maley and O Vandal. (2013). Host-directed therapeutics for tuberculosis: can we harness the host? Microbiol Mol Biol Rev 77:608–627.
35. Wallis RS and R Hafner. (2015). Advancing host-directed therapy for tuberculosis. Nat Rev Immunol 15:255–263.
36. Cohen SP, BL Peterlin, L Fulton, ET Neely, C Kurihara, A Gupta, J Mali, DC Fu, MB Jacobs *et al.* (2015). Randomized, double-blind, comparative-effectiveness study comparing pulsed radiofrequency to steroid injections for occipital neuralgia or migraine with occipital nerve tenderness. Pain 156:2585–2594.
37. de Gans J, D van de Beek and I European Dexamethasone in Adulthood Bacterial Meningitis Study. (2002). Dexamethasone in adults with bacterial meningitis. N Engl J Med 347:1549–1556.
38. Schutz C, AG Davis, B Sossen, RP Lai, M Ntsekhe, YX Harley and RJ Wilkinson. (2018) Corticosteroids as an adjunct to tuberculosis therapy. Expert Rev Respir Med 12: 881–891.
39. Scotland T R C o t T S o. (1957). PREDNISOLONE in the treatment of pulmonary tuberculosis: a controlled trial; a preliminary report by the Research Committee of the Tuberculosis Society of Scotland. Br Med J 2:1131–1134.
40. Dooley DP, JL Carpenter and S Rademacher. (1997). Adjunctive corticosteroid therapy for tuberculosis: a critical reappraisal of the literature. Clin Infect Dis 25:872–887.
41. Lavers KW and JC Roberts. (1959) The use of prednisone in primary tuberculosis in children. Tubercle 40:173–176.

42. Meintjes G, RJ Wilkinson, C Morroni, DJ Pepper, K Rebe, MX Rangaka, T Oni and G Maartens. (2010). Randomized placebo-controlled trial of prednisone for paradoxical tuberculosis-associated immune reconstitution inflammatory syndrome. AIDS 24:2381–2390.
43. Roehr B. (1998). Fomivirsen approved for CMV retinitis: first antisense drug. AIDS Treat News 7.
44. Hoy SM. (2017). Nusinersen: first global approval. Drugs 77:473–479.
45. Bajan S and G Hutvagner. (2020). RNA-based therapeutics: from antisense oligonucleotides to miRNAs. Cells 9:137.
46. Martinez FO and S Gordon. (2014). The M1 and M2 paradigm of macrophage activation: time for reassessment. F1000Prime Rep 6:13.
47. Chaussabel D, RT Semnani, MA McDowell, D Sacks, A Sher and TB Nutman. (2003). Unique gene expression profiles of human macrophages and dendritic cells to phylogenetically distinct parasites. Blood 102:672–681.
48. O'Connell R M, D S Rao and D Baltimore. (2012). microRNA regulation of inflammatory responses. Annu Rev Immunol 30:295–312.
49. Subuddhi A, M Kumar, D Majumder, A Sarkar, Z Ghosh, M Vasudevan, M Kundu and J Basu. (2020). Unraveling the role of H3K4 trimethylation and lncRNA HOTAIR in SATB1 and DUSP4-dependent survival of virulent *Mycobacterium tuberculosis* in macrophages. Tuberculosis (Edinb) 120:101897.
50. Emmrich S, A Streltsov, F Schmidt, VR Thangapandi, D Reinhardt and J H Klusmann. (2014). LincRNAs MONC and MIR100HG act as oncogenes in acute megakaryoblastic leukemia. Mol Cancer 13:171.
51. Han C, H Li, Z Ma, G Dong, Q Wang, S Wang, P Fang, X Li, H Chen *et al.* (2021). MIR99AHG is a noncoding tumor suppressor gene in lung adenocarcinoma. Cell Death Dis 12:424.
52. Brombacher F. (2000). The role of interleukin-13 in infectious diseases and allergy. Bioessays 22:646–656.
53. Nelms K, AD Keegan, J Zamorano, JJ Ryan and WE Paul. (1999). The IL-4 receptor: signaling mechanisms and biologic functions. Annu Rev Immunol 17:701–738.
54. Hernandez-Pando R, D Aguilar, ML Hernandez, H Orozco and G Rook. (2004). Pulmonary tuberculosis in BALB/c mice with non-functional IL-4 genes: changes in the inflammatory effects of TNF-alpha and in the regulation of fibrosis. Eur J Immunol 34:174–183.
55. Behar SM, CJ Martin, MG Booty, T Nishimura, X Zhao, HX Gan, M Divangahi and HG Remold. (2011). Apoptosis is an innate defense function of macrophages against *Mycobacterium tuberculosis*. Mucosal Immunol 4:279–287.
56. Chen M, H Gan and HG Remold. (2006). A mechanism of virulence: virulent *Mycobacterium tuberculosis* strain H37Rv, but not attenuated H37Ra, causes significant mitochondrial inner membrane disruption in macrophages leading to necrosis. J Immunol 176:3707–3716.
57. Gan H, J Lee, F Ren, M Chen, H Kornfeld and HG Remold. (2008). *Mycobacterium tuberculosis* blocks crosslinking of annexin-1 and apoptotic envelope formation on infected macrophages to maintain virulence. Nat Immunol 9:1189–1197.
58. Lerner TR, S Borel, DJ Greenwood, U Repnik, MR Russell, S Herbst, ML Jones, LM Collinson, G Griffiths and MG Gutierrez. (2017). *Mycobacterium tuberculosis* replicates within necrotic human macrophages. J Cell Biol 216:583–594.
59. Grab J, I Suarez, E van Gumpel, S Winter, F Schreiber, A Esser, C Holscher, M Fritsch, M Herb *et al.* (2019). Corticosteroids inhibit *Mycobacterium tuberculosis*-induced necrotic host cell death by abrogating mitochondrial membrane permeability transition. Nat Commun 10:688.
60. Berens HM and KL Tyler. (2011). The proapoptotic Bcl-2 protein Bax plays an important role in the pathogenesis of reovirus encephalitis. J Virol 85:3858–3871.
61. Carberry S, B D'Orsi, N Monsefi, M Salvucci, O Bacon, J Fay, M Rehm, D McNamara, EW Kay and JHM Prehn. (2018). The BAX/BAK-like protein BOK is a prognostic marker in colorectal cancer. Cell Death Dis 9:125.
62. Gaumer S, I Guenal, S Brun, L Theodore and B Mignotte. (2000). Bcl-2 and Bax mammalian regulators of apoptosis are functional in Drosophila. Cell Death Differ 7:804–814.
63. Gutta C, A Rahman, C Aura, P Dynoodt, EM Charles, E Hirschenhahn, J Joseph, J Wouters, C de Chaumont *et al.* (2020). Low expression of pro-apoptotic proteins Bax, Bak and Smac indicates prolonged progression-free survival in chemotherapy-treated metastatic melanoma. Cell Death Dis 11:124.
64. Kulsoom B, TS Shamsi, NA Afsar, Z Memon, N Ahmed and SN Hasnain. (2018). Bax, Bcl-2, and Bax/Bcl-2 as prognostic markers in acute myeloid leukemia: are we ready for Bcl-2-directed therapy? Cancer Manag Res 10:403–416.
65. Naseri MH, M Mahdavi, J Davoodi, SH Tackallou, M Goudarzvand and SH Neishabouri. (2015). Up regulation of Bax and down regulation of Bcl2 during 3-NC mediated apoptosis in human cancer cells. Cancer Cell Int 15:55.
66. Cooper A M, K D Mayer-Barber and A Sher. (2011). Role of innate cytokines in mycobacterial infection. Mucosal Immunol 4:252–260.
67. Zhang Q, TC Chao, VS Patil, Y Qin, SK Tiwari, J Chiou, A Dobin, CM Tsai, Z Li *et al.* (2019). The long noncoding RNA ROCKI regulates inflammatory gene expression. EMBO J 38:e100041.
68. Feyder M and L A Goff. (2016). Investigating long noncoding RNAs using animal models. J Clin Invest 126:2783–2791.
69. MacMicking JD, RJ North, R LaCourse, JS Mudgett, SK Shah and CF Nathan. (1997). Identification of nitric oxide synthase as a protective locus against tuberculosis. Proc Natl Acad Sci U S A 94:5243–5248.
70. Liu B, L Sun, Q Liu, C Gong, Y Yao, X Lv, L Lin, H Yao, F Su *et al.* (2015). A cytoplasmic NF-kappaB interacting long noncoding RNA blocks IkappaB phosphorylation and suppresses breast cancer metastasis. Cancer Cell 27:370–381.
71. Chu C, K Qu, FL Zhong, SE Artandi and HY Chang. (2011). Genomic maps of long noncoding RNA occupancy reveal principles of RNA-chromatin interactions. Mol Cell 44:667–678.
72. Hasegawa Y, N Brockdorff, S Kawano, K Tsutui, K Tsutui and S Nakagawa. (2010). The matrix protein hnRNP U is required for chromosomal localization of Xist RNA. Dev Cell 19:469–476.
73. Huarte M, M Guttman, D Feldser, M Garber, MJ Koziol, D Kenzelmann-Broz, AM Khalil, O Zuk, I Amit *et al.* (2010). A large intergenic noncoding RNA induced by p53

mediates global gene repression in the p53 response. Cell 142:409–419.
74. Hu J, Z Chen, D Xia, J Wu, H Xu and Z Q Ye. (2012). Promoter-associated small double-stranded RNA interacts with heterogeneous nuclear ribonucleoprotein A2/B1 to induce transcriptional activation. Biochem J 447:407–416.
75. Wang G, Q Xiao, Z Luo, S Ye and Q Xu. (2012). Functional impact of heterogeneous nuclear ribonucleoprotein A2/B1 in smooth muscle differentiation from stem cells and embryonic arteriogenesis. J Biol Chem 287:2896–2906.
76. Zhang K, ZM Shi, YN Chang, ZM Hu, HX Qi and W Hong. (2014). The ways of action of long non-coding RNAs in cytoplasm and nucleus. Gene 547:1–9.
77. Kotzin JJ, SP Spencer, SJ McCright, DBU Kumar, MA Collet, WK Mowel, EN Elliott, A Uyar, MA Makiya *et al.* (2016). The long non-coding RNA Morrbid regulates Bim and short-lived myeloid cell lifespan. Nature 537:239–243.
78. Huang W, B Thomas, RA Flynn, SJ Gavzy, L Wu, SV Kim, JA Hall, ER Miraldi, CP Ng *et al.* (2015). DDX5 and its associated lncRNA Rmrp modulate TH17 cell effector functions. Nature 528:517–522.
79. Zgheib C, MM Hodges, J Hu, KW Liechty and J Xu. (2017). Long non-coding RNA Lethe regulates hyperglycemia-induced reactive oxygen species production in macrophages. PLoS One 12:e0177453.

Address correspondence to:
Frank Brombacher, PhD
International Centre for Genetic Engineering and Biotechnology (ICGEB)
Department of Pathology
Cape Town Component
Cape Town 7925
South Africa

E-mail: Frank.Brombacher@icgeb.org

Reto Guler, PhD
Division of Immunology
Department of Pathology
Institute of Infectious Diseases and Molecular Medicine (IDM)
University of Cape Town
International Centre for Genetic Engineering and Biotechnology (ICGEB)
Cape Town Component
Cape Town 7925
South Africa

E-mail: reto.guler@uct.ac.za

Received for publication March 9, 2022; accepted after revision May 5, 2022; Published Online July 27, 2022.